Available online at www.sciencedirect.com
ScienceDirect
Catalysis Today 136 (2008) 84–92
CATALYSIS TODAY
www.elsevier.com/locate/cattod

Coupled theoretical and experimental analysis of surface coverage effects in Pt-catalyzed NO and O_2 reaction to NO_2 on Pt(1 1 1)

A.D. Smeltz [a], R.B. Getman [b], W.F. Schneider [b,c,*], F.H. Ribeiro [a,*]

[a] School of Chemical Engineering, Purdue University, West Lafayette, IN 47907, United States
[b] Department of Chemical and Biomolecular Engineering, University of Notre Dame, Notre Dame, IN 46556, United States
[c] Department of Chemistry and Biochemistry, University of Notre Dame, Notre Dame, IN 46556, United States

Available online 5 March 2008

Abstract

Batch reactor results and analysis are reported for the reaction of NO with O_2 to form NO_2 over a Pt(1 1 1) single crystal at atmospheric pressure. The apparent activation energy and NO, O_2, and NO_2 reaction orders are found to be 80 kJ mol^{-1}, 1.3, 1, and −2 and are comparable to previous studies on supported Pt catalysts which take inhibition by the product NO_2 into account. The absolute rates on a per Pt atom basis are the highest yet reported 0.34 ± 0.02 s^{-1}, at 300 °C, 73 ppm NO, 27 ppm NO_2 and 5% O_2. Auger electron spectroscopy and X-ray photoelectron spectroscopy are used to show that the surface chemisorbed oxygen coverage under reaction conditions is 0.76 ± 0.06 ML, consistent with a coverage controlled by NO_2 dissociation. DFT calculations are used to compare the stability of possible surface intermediates on a clean Pt(1 1 1) surface with those on a $p(\sqrt{3} \times \sqrt{3})$-2O (2/3 ML) ordering surface. In contrast to the clean surface, O_2 adsorption and dissociation are endothermic at 2/3 ML oxygen, but a peroxynitrite intermediate OONO* is slightly stable and may provide an alternative, associative pathway to NO_2 formation that is consistent with the observed first order reaction kinetics in O_2.

Keywords: NO oxidation; Pt catalyst; Kinetics; AES; XPS; DFT; Peroxynitrite

1. Introduction

The catalytic oxidation of NO to NO_2:

$$NO(g) + 1/2O_2(g) \leftrightarrow NO_2(g) \quad (1)$$

is a key reaction in technologies to sense [1] and to remediate [2,3] NO_x from lean exhaust gas streams. NO oxidation to NO_2 is the first step in NO_x storage as implemented in lean NO_x traps (LNTs), and the NO/NO_2 ratio as controlled via reaction (1) has a large effect of the rate of NO_x selective catalytic reduction (SCR). Because of its small heat of reaction (−57 kJ/mol) the equilibrium reaction shifts from product to reactant dominated at several hundred Celsius, and thus there is much interest in developing active and stable low temperature catalysts. The reaction is commonly catalyzed by Pt dispersed on an oxide support, and the mechanism of this reaction has been the topic of experimental [4–14] and computational research [11,15–19]. Early experimental evidence pointed to an increase in intrinsic catalytic activity with increasing Pt particle size [4,5], and more recent experimental results confirm this behavior [12]. Kinetic measurements on supported catalysts indicate that the reaction is first order in NO and O_2 and negative first order in NO_2 [11,12]. Experiments further indicate that activity is associated with high coverages of surface oxygen on the Pt metal particles but that complete oxidation of the particle surface results in catalyst deactivation [12]. NO_2 is well known to be more effective than molecular O_2 at dosing atomic oxygen to single crystal Pt surfaces [20–22], consistent with the observation of high oxygen coverages and inhibition of the catalytic oxidation reaction in the presence of the oxidation product, NO_2.

These catalytic observations have been explained by a mechanism in which oxygen is the most abundant surface intermediate and is in equilibrium with gas-phase NO_2 [12]:

$$NO_2(g) + 2* \leftrightarrow NO* + O* \quad (2)$$

In this model, net NO oxidation is achieved by coupling reaction (2) to separate NO and O_2 adsorption and dissociation

* Corresponding authors.
E-mail addresses: wschneider@nd.edu (W.F. Schneider), fabio@purdue.edu (F.H. Ribeiro).

0920-5861/$ – see front matter © 2008 Elsevier B.V. All rights reserved.
doi:10.1016/j.cattod.2007.12.139

steps

$$NO(g) + * \leftrightarrow NO* \quad (3)$$

$$O_2(g) + * \rightarrow \ldots \quad (4)$$

First-principles density functional theory (DFT) simulations do indicate that the conversion of NO* to NO_2* is energetically feasible only under conditions in which a Pt(1 1 1) terrace is highly O covered, weakening the Pt–O bonds by destabilizing lateral interactions with neighbor O atoms [16,18]. Calculations further indicate that very small Pt particles are highly susceptible to complete oxidation [23,24].

The results to date leave key mechanistic questions unanswered about the generation and nature of the highly oxygen covered Pt surface, its interactions with NO and O_2, and the role of these intermediates in NO oxidation catalysis. In this work, we report atmospheric-pressure batch reactor results for the rate of catalytic NO oxidation over a Pt(1 1 1) single crystal. We show that the reaction orders of NO oxidation are similar on this 1 cm diameter large single crystal to that on a supported nanosized Pt particle. Further, we use *ex situ* X-ray photoelectron spectroscopy (XPS) and Auger electron spectroscopy (AES) to estimate surface oxygen coverage under reaction conditions. Building on these results, we use DFT calculations to determine the structure and stability of potential reaction intermediates on a Pt(1 1 1) surface at oxygen coverages comparable to those experimentally observed. We find that NO and O_2 adsorption are inhibited at high coverages relative to the pristine surface, but that co-adsorption as an OONO* intermediate enhances binding. The formation of this intermediate may be important in facilitating the dissociation of O_2.

2. Experimental and computational details

2.1. UHV analysis chamber and atmospheric pressure batch reactor cell

Kinetic measurements were carried out on a combined atmospheric batch reactor and ultra-high vacuum (UHV) analytical chamber which allows for *in vacuo* sample transfer between the reactor and analytical chamber. The 0.96 L batch reactor system consists of a stainless steel reaction chamber and two gas circulation pumps (Metal Bellows, MB-21) which circulate gas within the reactor and to a Fourier transform infrared spectrometer (FTIR) equipped with a three meter path length gas cell for quantitative measurement of NO and NO_2 concentrations in the reactor. The absolute error in the measurements was ±2 ppm or less for both gases over the range studied. The reaction gases are introduced into the reactor one at a time using a gas manifold while monitoring the total pressure in the reactor using a MKS Baratron pressure transducer which has an accuracy of ±0.1 Torr. The UHV chamber had a base pressure of 7×10^{-10} Torr and contains an X-ray gun, a PHI 15-255G double pass cylindrical mirror analyzer (CMA) equipped with an electron gun for X-ray photoelectron (XPS) and Auger electron spectroscopy (AES), a UTI-100C mass spectrometer (MS), ion gun, and low energy electron diffraction (LEED). AES spectra were acquired in differential mode, using a PHI lock-in amplifier for analogue differentiation.

2.2. Pt(1 1 1) sample

The Pt(1 1 1) single crystal (Mateck GmbH) with an orientation accuracy of $<0.5^\circ$ was mounted to the sample holder by two stainless steel pins spot welded to the side of the crystal. The sample temperature was measured by a K-type thermocouple spot welded to the side of the crystal. Controlled heating was accomplished by passing electrical current directly through the sample via the steel pins using an Electronic Measurements Inc., TCR dc power supply which was regulated using a Eurotherm 2408 PID controller. The crystal was prepared by repeated 1 keV Ar^+ sputtering at ambient temperature, exposure to 1×10^{-5} Torr O_2 at 500 °C and annealing at 750 °C until no impurities such as Si, C, Ca, or O were found using AES or XPS and a sharp (1 1 1) diffraction pattern was seen by LEED. The turnover rate (TOR) was calculated based on the geometric surface area of the crystal face, 0.64 cm^2 and using a surface density of Pt atoms of 1.51×10^{15} cm^{-2}. Only the front face of the crystal was assumed to be active since the reverse side did not receive any sputter cleaning.

2.3. Analysis of batch data

The batch experiments were carried out by introducing N_2, O_2, 300 ppm NO_2/N_2 mixture, and finally 300 ppm NO/N_2 mixture to 760 Torr one at a time into the reactor while the catalyst remained at the reaction temperature. Gases were of Matheson purity grade except for N_2 which was from LN_2 boil off. Batch reactions typically lasted about 20 min after the gases were given several minutes to mix. The batch data ([NO] and $[NO_2]$ vs. time) was analyzed by first numerically smoothing and differentiating [NO] or $[NO_2]$ in order to get the overall rate of reaction, then subtracting the homogeneous gas phase reaction rate contribution to the overall rate, and finally correcting for approach to equilibrium such that for every batch reaction a set of forward TOR on Pt(1 1 1) versus [NO] and $[NO_2]$ were obtained. To account for the approach to equilibrium, the stoichiometric number for the rate-determining step (RDS) in relation to the overall reaction stoichiometry, $2NO + O_2 \rightarrow 2NO$, must be known. We believe that the RDS is the adsorption of O_2 and therefore the overall rate on Pt can be converted to the forward rate by dividing by $(1 - \beta)$, where β equals $(P^2_{NO_2}/P^2_{NO}P_{O_2}K_{eq}(T))$. $K_{eq}(T)$ represents the equilibrium constant for the overall reaction and is calculated at the catalyst temperature, T. In a previous publication from our group [11], the approach to equilibrium was derived inconsistently. The form above was pointed out to us by Weiss and Iglesia [25]. The gas phase NO oxidation kinetic model [26] was verified in separate experiments. Before data were collected for analysis, batch reactions were run until subsequent batch reactions gave similar results indicating the Pt(1 1 1)

activity had stabilized in the reaction mixture. Batch experiments were designed such that reaction orders and the apparent activation energy (E_a) could be directly determined from the data using linear regression. Ten to 20 batch reactions were used to determine each kinetic parameter many times at different conditions. Representative values of each parameter are reported here.

2.4. Ex situ measurements by AES and XPS

After the final batch reaction, the sample was cooled to <40 °C in the reaction mixture before the reactor was evacuated to 5×10^{-5} Torr at which time the sample was transferred to the analysis chamber in order to check for impurities and measure the oxygen coverage using AES and also to check for Pt oxidation by XPS. Sample cooling, evacuation, transfer to UHV, and initiation of AES took about 10 min. Oxygen coverage was determined by measuring the peak-to-peak heights of the Pt_{235} and O_{507} Auger transitions in the differentiated spectra and comparing the ratio to the calibration curve published by Saliba et al. [27]. Saliba et al. also used a double pass CMA with 3 kV electron gun energy. Previous attempts to calibrate our AES measurements by means of the well known 0.25 ML saturation coverage using O_2 [28] were unsuccessful, probably due to the low sticking coefficient of O_2 (~0.05) on clean Pt(1 1 1) [29] combined with clean off reactions with trace amounts of CO and H_2 in the analysis chamber. Unfortunately, trace H_2 and CO was unavoidable in our situation due to the repeated exposure of the UHV chamber to the atmospheric pressure reaction chamber which typically had a pressure of 5×10^{-5} Torr during sample transfer after reaction. Attempts at calibrating with NO_2, which saturates the surface with 0.75 ML of atomic oxygen at 400 K [21] were also unsuccessful due to a lack of a microcapillary doser connected to the leak valve, which avoids efficient NO_2 pumping, by the walls of the UHV chamber. Desorption of oxygen caused by the 3 kV electron beam was also an issue. It was determined that the electron beam was causing a linear decrease of ~0.05 ML oxygen per minute. AES measurements presented here lasted less than 1 min with the O_{507} region scanned in the first 20 s after initial exposure to the electron beam since the Pt_{235} intensity is known to change minimally due to attenuation from the oxygen overlayer [27]. Using this procedure, it was estimated that negligible oxygen desorbed during the experiment and therefore no correction was made due to desorption from the electron beam especially since the error in using the calibration from Saliba et al. [27] is likely to be significantly larger. XPS experiments were performed using a Mg anode, 300 W filament power, 15 kV acceleration voltage, and a pass energy of 50 eV in order to maximize signal to noise ratio as well as keep the full width half maximum (FWHM) of the Pt_{4f} peaks as narrow as possible in order to maximize our ability to see Pt oxidation if it occurred. The angle of the Pt(1 1 1) surface normal with respect to the CMA was about 30°. Spectra were analyzed using CasaXPS software (http://www.casaxps.com) using a hybrid Doniach-Sunjic, summed Gauss-Lorentzian function for the Pt peaks.

2.5. Computational details

DFT calculations were performed with the Vasp code [30]. Electron cores were simulated with the PAW method [31,32], planes waves included to a cut-off of 400 eV, and the electron exchange and correlation interactions were treated using the PW91 implementation of the generalized gradient approximation (GGA) [33,34].

Pt(1 1 1) surfaces were simulated with periodic four-layer 4Pt × 4Pt and 3Pt × 3Pt supercells and separated from vertical images by five equivalent layers (about 14 Å) of vacuum space. Atoms in the bottom layers of the supercells were held fixed in their calculated bulk positions, and all remaining atoms were allowed to relax. The first Brillouin zones were sampled using Monkhorst-Pack [35] k-point grids of $6 \times 6 \times 1$ and $8 \times 8 \times 1$, respectively. Atoms and molecules were allowed to adsorb only to the top Pt layer. Test calculations show that the effect of spin polarization is negligible for all adsorbates considered except for O_2, which is stabilized by at most 70 meV with its inclusion. All extended surface energies reported here are for non-spin polarized adsorbates. Adsorbate vibrational frequencies and zero point energies were computed within the harmonic oscillator approximation by two-sided finite differences in the DFT gradients. All atoms within the adsorbate as well as its immediate neighbor Pt were perturbed by ±0.01 Å in all three Cartesian directions, and modes were determined by diagonalization of the Hessian matrix. Modes for all adsorbates except OONO* were computed at low coverage, i.e. with one adsorbate per 16 surface Pt. Bound OONO* does not exist at low coverage, so vibrational analysis on it was performed on one OONO* co-adsorbed with 6 O over 9 Pt. Other than the Pt nearest the adsorbate, lattice Pt and O were not included in the vibrational mode analyses. All other computational details are as described in Ref. [18].

3. Experimental results

3.1. System validation

Because of the small amount of Pt available for reaction, care was taken to correct for background activity resulting from reaction in the gas phase as well as the possibility of reaction on the hot stainless steel pins used for the sample holder. The homogenous gas phase NO oxidation reaction was accounted for in our analysis since it was found that the rate of reaction in the gas phase was similar to that on Pt(1 1 1) at the conditions tested. The rate in the gas phase represented 10–67% of the overall rate of the reaction. The kinetic model used [26] was verified using separate batch reaction experiments with no catalyst present. The accuracy of rates in the model was better than ±0.03 s^{-1} when normalized to the Pt(1 1 1) surface at the conditions studied. This also verified that the reactor walls were not contributing significantly to the overall rate of reaction, however significant treatment in NO_2 was needed to passivate the stainless steel to prevent further reaction with NO_2. To verify that the hot steel pins used for sample mounting were not contributing to the rate of reaction, a piece of 316 stainless steel

foil was mounted onto the sample holder and tested for activity at 300 °C. No activity was observed on the foil. In fact, a slight decrease in the measured rate as compared to the one without the foil occurred due to a slight heating from of the gas phase from 22 °C to 24 °C since the apparent activation energy for the gas phase NO oxidation reaction is negative.

External mass transfer limitations were also checked for using the Chilton-Colburn J factor heat and mass transfer analogy [36] in a series of heat transfer tests. At the conditions used in this study, it was found that the rate of mass transfer of NO to the surface was at least one order of magnitude above the rate of reaction and therefore we are confident that the kinetics are not influenced by external mass transfer. Turnover rates (TOR) on Pt up to four times higher have also been measured in this system than the TOR reported here further verifying that the kinetics reported here were not limited by mass transfer. Internal heat and mass transfer limitations are not relevant in this case since the Pt(1 1 1) single crystal is not porous.

Finally, the effect of thermocouple position on the side of the crystal as well as inevitable variations in spot welding of the crystal to the sample holder was tested by remounting the crystal several times and measuring the activity. It was found that the Pt(1 1 1) TOR was not sensitive to either of these issues compared to the day-to-day variability of the catalyst activity.

3.2. Reaction orders and apparent activation energy

Before data were collected for kinetic analysis, the catalyst was allowed to stabilize by running batch reactions until subsequent reactions gave similar results. Once the catalyst was stable, various conditions were run for each kinetic parameter in a non-sequential fashion while periodically going back to the original condition to check for deactivation. It was found that once the catalyst initially stabilized, very little further deactivation occurred during the experiments and therefore no deactivation correction was needed. Stabilized rates were typically 2–2.5 times lower than the initial rate. In general, the stabilized catalyst activity was very repeatable on a day-to-day basis. Fig. 1 shows two examples of typical stabilization profiles for Pt(1 1 1) from different days. Since no Pt oxidation was observed by AES or XPS, it is not clear as to why the catalyst deactivates by this amount, though it is possible that small amounts of surface impurities may have been to blame, see Section 3.3.

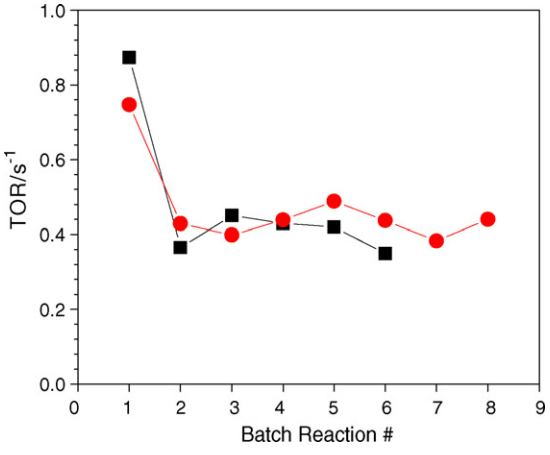

Fig. 1. Stabilization of Pt(1 1 1) at 300 °C, 76 ppm NO, 24 ppm NO_2 and 5% O_2 as a function of batch reactions. The first reaction lasted 90 min whereas each subsequent reaction lasted ~25 min. Symbols represent different days.

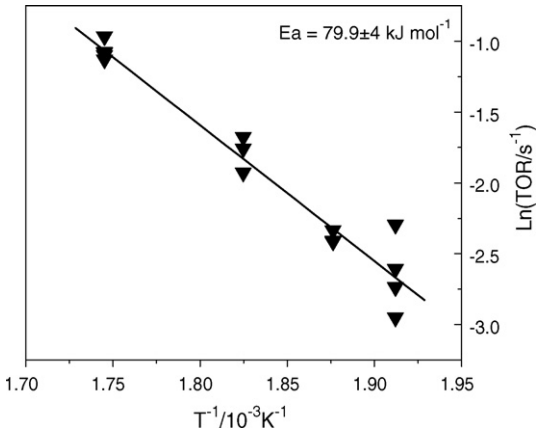

Fig. 2. Representative Arrhenius plot for the NO oxidation reaction on Pt(1 1 1). Conditions were 250–300 °C, 5% O_2, 73 ppm NO, and 27 ppm NO_2. Error represents the 95% confidence interval from the regression.

Figs. 2 and 3 show reaction orders and the apparent activation energy (E_a) for the NO oxidation reaction on Pt(1 1 1), which represent the average values measured over the course of the study. Since the data were collected by running batch reactions, for a given set of 15–20 batch reactions, many values of the kinetic parameter being studied could be generated. Reaction orders and activation energy were also measured at different sets of conditions on different days to ensure the validity of each parameter. However, the range of conditions was fairly limited in order to keep the ratio of the rate on Pt to the rate in the gas phase as high as possible. It was found that the oxygen order and E_a were fairly consistent during the study with average values of approximately +1 and 80 kJ/mol, respectively, however the NO and NO_2 orders varied significantly. The NO order was measured to be anywhere from

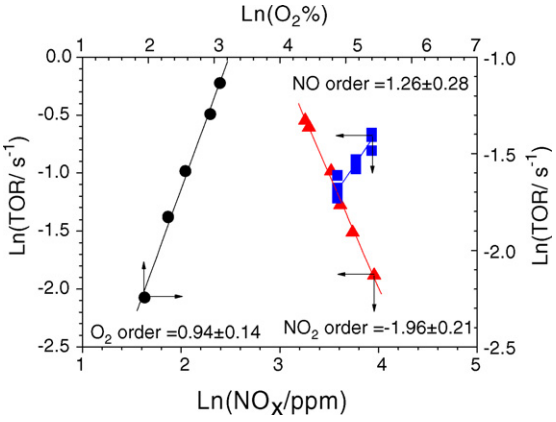

Fig. 3. Reaction order dependence for the NO oxidation reaction on Pt(1 1 1). Conditions for NO order (■) were 300 °C, 14 ppm NO_2, and 50–65 ppm NO, for NO_2 order (▲) 335 °C, 5%O2, 78 ppm NO, and 27–52 ppm NO_2, and for O_2 order (●) 285 °C, 52 ppm NO, 18 ppm NO_2, and 7–22% O_2. Error represents the 95% confidence interval from the regression.

1.2 ± 0.3 to 1.7 ± 0.2, with the average order of 1.3 and measurements of the NO_2 order varied from -1.3 ± 0.2 to -2 ± 0.2, with the vast majority of the data indicating an order of -2. The errors reported here represent the standard deviation from the individual data set. No relationship in the variation in the NO and NO_2 orders to the reaction conditions used were found. The kinetic parameters presented in Figs. 2 and 3 represent the result from the regression analysis on the data shown in the figures and are representative of the average of the values measured as well as typical error in the regression analysis. Fig. 4 compares the average values of the NO and NO_2 orders to batch reactor data taken after stabilization and shows that the averaged NO and NO_2 orders describe the kinetics on Pt(1 1 1) very well. Fig. 4 also compares the batch data to the kinetics reported by Mulla et al. [11].

Previous NO oxidation kinetic studies on supported Pt can be lumped into two groups: those who either ignored kinetic inhibition of the product NO_2 or dismissed it as a artifact of Pt oxidation by not including NO_2 in the reactor feed, [13,37] for example, and therefore did not include NO_2 in their global kinetic model, and those who recognized the inhibition effect of NO_2 and therefore included it into their feed [10,11], for example. In plug flow reactor (PFR) studies, it is vital that all reactants and products are fed in excess if differential conditions are to be assumed. Mulla et al. [11] showed that apparent activation energies and reaction orders will appear to be half of their actual value if the product NO_2 is not included in the feed. Mulla et al. measured an activation energy of ~80 kJ/mol and NO, O_2, and NO_2 orders of approximately +1, +1, and −1, respectively where as Ji et al. [13] and Hauptmann et al. [14] both reported E_a, NO and O_2 orders roughly half of these in agreement with the arguments presented by Mulla et al. [11].

In this batch reactor study using Pt(1 1 1) study we found an E_a of 80 kJ mol^{-1} and NO, O_2 and NO_2 reaction orders of 1.3, 1, and −2, respectively. The E_a and O_2 order are in great agreement with those found by Mulla et al. [11], however the

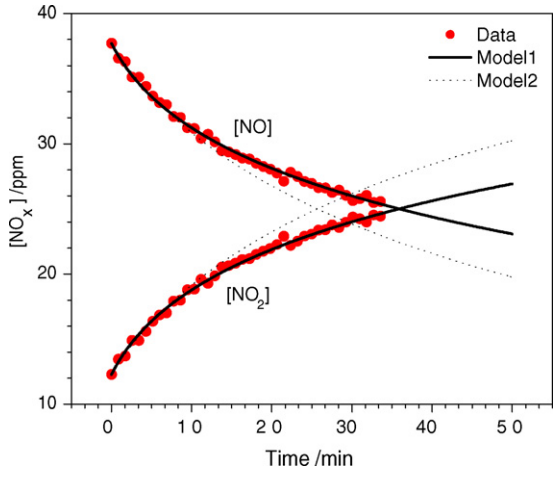

Fig. 4. Comparison of batch data to two kinetic models. Model 1 assumes an NO and NO_2 orders shown in Fig. 3, Model 2 assumes +1 and −1 for NO and NO_2 orders, respectively, and both models take into account the background homogeneous gas phase reaction. Four out of five batch data points are not included for clarity. Conditions were 50 ppm NO initially, 5% O_2, and 300 °C.

NO and NO_2 orders show some deviation. The data clearly indicates that NO_2 inhibits the NO oxidation activity significantly. Several possibilities for the deviation of the NO and NO_2 orders exist if we are to believe that the true orders are likely closer to +1 and −1, respectively. One possibility is a repeatable, reversible deactivation, which began at the beginning of every batch reaction and was due to Pt oxidation or contamination by a volatile surface impurity, both of which are reversed upon evacuation of the reaction gases in between batch reactions since the data in Fig. 1 indicates that continuous irreversible deactivation was not occurring. Both possibilities are considered further in Section 3.3. Another possibility is error in the subtraction of the gas phase NO oxidation reaction. A sensitivity analysis indicated that both NO and NO_2 orders can be very sensitive to the gas phase model under certain conditions, showing a deviation up to −0.2 and +0.2, respectively after a 3% decrease (+5 °C) in the gas phase rate constant. The O_2 order and E_a were found to be virtually insensitive to the same change in the gas phase rate constant. However, the sensitivity analysis represents worse case scenarios and in fact subsequent experiments such as the data shown in Fig. 4, in which the experiments were run such that the gas phase rate was almost negligible compared to the rate on the Pt(1 1 1) and still fit the kinetics reported in Fig. 3. Even though some error was probably introduced by subtraction of the gas phase rate of reaction in this study, it is concluded that this error is likely not the main cause of the deviation of the NO and NO_2 orders from their expected values of +1 and −1, respectively.

Finally, we can compare NO oxidation TOR on Pt reported in literature versus the rates found on Pt(1 1 1). Of all the TOR reported in literature for NO oxidation, Crocoll et al. [38] reported the highest TOR on their Pt/Al_2O_3 catalyst with an average particle diameter of 200 nm as measured by SEM. Converting their data at 300 °C to 73 ppm NO, 27 ppm NO_2 and 5% O_2 using NO, O_2, and NO_2 orders of +1, +1, and −1, respectively, the TOR on their catalyst was ~0.2 s^{-1}. The TOR on Pt(1 1 1) reported in Fig. 2 at these conditions is 0.34 ± 0.02 s^{-1} where the error represents the standard deviation of six measurements. Crocoll et al. [38] used PXRD to prove the existence of crystalline Pt particles, indicated by (1 1 1) and (2 0 0) peaks as expected with such a large Pt particle size. The TOR data of Crocoll and the Pt(1 1 1) data presented here are in reasonable agreement which is expected since the (1 1 1) surface represents the most thermodynamically stable Pt surface and is the preferred crystallographic surface orientation under the limit of large particle size.

3.3. Ex situ characterization by AES and XPS

3.3.1. Surface impurities

Performing catalytic studies on exposed low surface area materials such as single crystals are inherently problematic due to surface contamination from within the bulk of the crystal or from the environment. AES was used to determine if any impurity contaminated the Pt(1 1 1) surface during the kinetic study. No typical impurities from the bulk of the crystal such as Si/SiO_2, S or Ca were found after reaction, however it must be

noted that Br was found after reaction evidenced by AES peaks at 55 eV, 101 eV, and 108 eV and the Br_{3p} doublet in XPS. It was found that the Br contamination was coming from the NO_2 cylinder used in the experiments. Comparing the O_{1s} and Br_{3p} intensities using XPS and knowing the oxygen coverage by AES, it was estimated that the Br coverage was 0.07 ± 0.01 ML when the Pt(1 1 1) was cooled in reaction mixture and <0.03 ML when the Pt(1 1 1) was kept at 300 °C during evacuation. The error bars represent the standard deviation of many measurements and indicate that the contamination was virtually the same on a day-to-day basis. No desorption of Br was observed due to interaction with the electron beam. Separate experiments starting with contaminated Pt(1 1 1) with ~0.07 ML and heating in vacuum to 300 °C for 1 min showed that ~90% of the Br desorbed from the surface. Therefore, we believe that the coverage of Br during the kinetic experiments was likely <0.07 ML. A relatively small amount of Br on the surface caused more deactivation (2–2.5 times) than predicted by simple site blocking alone. It is very likely that the Br contamination caused a reversible, repeatable deactivation during the experiments which could explain why the NO order and especially the NO_2 order are different than previous studies on supported Pt. Evacuation between each experiment desorbed most of the Br and then when the next reaction was started Br would have slowly re-deposited on the surface. This would be a fairly repeatable process which was missed when comparing TOR from subsequent batch reactions. Current work is ongoing in order to determine the effect of the Br on the NO oxidation kinetics and the results will reported in future publications.

3.3.2. *Oxygen coverage after reaction*

AES was used *ex situ* after the last batch reaction by first quenching the catalyst in the reaction mixture to <40 °C, evacuating, and finally transferring to the analysis chamber and performing the measurement. The average coverage from four experiments was 0.76 ± 0.07 ML (error represents one standard deviation) after quenching in the reaction mixture of 5% O_2, 56 ppm NO and 40 ppm NO_2. This is identical to the saturation coverage of atomic oxygen using NO_2 at low pressures and at temperatures above 400 K [21,39] and therefore suggests that the product NO_2 is controlling oxygen coverage on surface rather than the reactant O_2. This explains the NO_2 inhibition found in the kinetic experiments since the NO_2 would adsorb on the surface depositing a high coverage of atomic oxygen, which would then inhibit molecular O_2 adsorption due to repulsive interactions with the atomic oxygen. Current work using *in situ* XPS under reaction conditions will offer a better look at the surface conditions under NO oxidation reaction conditions since it is not clear as to how much quenching the Pt(1 1 1) in the reaction alters the surface coverage of oxygen.

Comparison of the Pt_{4f} region by XPS on clean Pt(1 1 1) and after quenching in the reaction mixture to <40 °C indicated that no measurable Pt oxidation occurred. The FWHM of the Pt_{4f} peaks were 1.3 eV on clean Pt which is narrow enough such that a small shoulder ~3.7 eV higher in binding energy due to Pt^{+2} or Pt^{+4} compared to Pt^0 [40] would have been observed if the surface Pt was oxidized. Only an increase in the FWHM of 0.1 eV was observed which was expected to be due to interaction with the oxygen overlayer and the peak position of the $Pt_{4f7/2}$ and $Pt_{4f5/2}$ peaks remained at 71 eV and 74.3 eV, respectively. This result combined with measurements by AES both indicate that Pt(1 1 1) did not significantly oxidize under NO oxidation reactions in the time scale of the kinetic experiments which typically lasted 8–10 h and therefore we can rule out deactivation by Pt oxidation as a possible explanation for the initial deactivation shown in Fig. 1 as well as the deviation of the NO and NO_2 orders.

4. Computational results

A key challenge in DFT simulation of NO oxidation intermediates on Pt is selection of an appropriate surface model and oxygen coverage. In this work we compare a low O coverage Pt(1 1 1) surface, modeled using a 4×4 supercell, with higher O coverage ones as suggested by the experimental results. The AES observations indicate oxygen coverage under reaction conditions of 0.76 ± 0.06 ML. We select the $p(\sqrt{3} \times \sqrt{3})$-2O ordering [41] to represent this surface (Fig. 5b), which has a 2/3 ML O coverage slightly below that observed experimentally. Repulsive interactions between O atoms are minimized at this coverage by ordering on FCC sites in a hexagonal pattern. According to our DFT results, this is the highest O coverage consistent with catalytic NO oxidation to NO_2; higher coverages or different arrangements (such as a mix

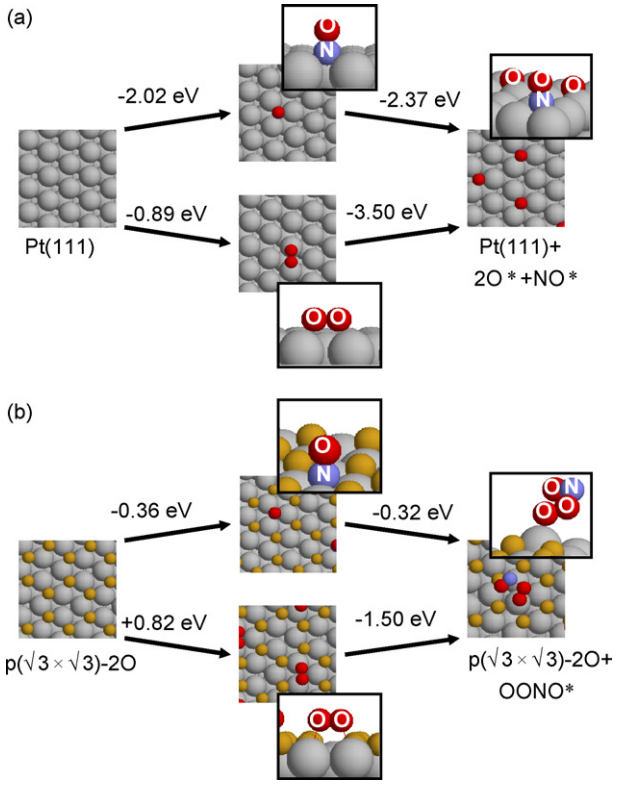

Fig. 5. NO and O_2 independent (left) and cooperative (right) adsorption energies ($\Delta H_{ads} = \Delta E^{DFT} + \Delta E^{ZP}$) on clean Pt(1 1 1) (a) and on the 2/3-ML O $p(\sqrt{3} \times \sqrt{3})$-2O ordering (b) at 0 K.

of FCC and HCP occupancies [42,43]) are calculated to be thermodynamically unstable to loss of O_2 to the gas-phase and thus are not consistent with catalytic NO oxidation. We represent this surface using a 3×3 Pt(1 1 1) supercell containing six surface O. For example, adding one more oxygen to this surface, to attain coverage of 0.78 ML, is endothermic with respect to gas-phase O_2 by 0.56 eV.

We first compute the binding energies of O_2 and NO on both the clean and 2/3 ML model surfaces. After independent adsorption, NO and O_2 are allowed to interact within their immediate surface environment to test for the formation of potential intermediates leading to NO_2 formation. Results are displayed in Fig. 5.

As shown in Fig. 5a, both NO and O_2 adsorb exothermically in isolation to clean Pt(1 1 1). NO prefers the threefold FCC site on Pt(1 1 1) at low coverage [18]. Molecular O_2 adsorbs more weakly and side-on to Pt(1 1 1), either in a top-bridge-top (TBT, Fig. 5a) configuration or a top-FCC-bridge (TFB) one [44,45]. These configurations are nearly isoenergetic regardless of the O coverage, as long as the amount of bound O_2 is small compared to that of bound O. Dissociation of O_2* to two O* is 1.80 eV exothermic at low coverage. Allowing NO and O_2 to co-adsorb within the 4×4 supercell does not change this energetic preference for O_2 dissociation, and the lowest energy arrangement remains NO* and O* adsorbed on separate FCC sites. Formation of NO_2* from NO* and O* is endothermic by 0.8 eV, thus showing the preference of low coverage Pt(1 1 1) for dissociation products over oxidation products.

Fig. 5b contrasts these behaviors on the $p(\sqrt{3} \times \sqrt{3})$-2O surface. NO and O_2 independent adsorption is energetically much less favorable than on the clean surface, indicated by the increase in adsorption energies to −0.36 eV and +0.82 eV, respectively. While a metastable adsorbed O_2 state can be identified, O_2 is further removed from the Pt surface than at low coverage, and binding is *endothermic* relative to gas-phase O_2. Molecular O_2 is thus expected to be present at low coverage and only transiently on this surface. Dissociation of O_2* to two O* is further endothermic by 0.49 eV. NO continues to prefer to adsorb molecularly at FCC sites, but with binding energy greatly reduced due to the sharing of Pt atoms with surface O*.

Association of NO and O_2 on this high coverage surface has the remarkable effect of actually *enhancing* the adsorption energies of both species. Co-adsorbed near the same vacant FCC sites, these two combine to form a bound OONO* complex similar in connectivity but with greater OO-NO bond length (1.814 Å) than the well known peroxynitrite anion, $OONO^{*-}$ (1.37 Å calculated at the B3LYP/6-311 + G* level [46]). The *cis* conformation is 0.2 eV lower in energy than the *trans*. The *cis*-OONO* intermediate binds O-down atop Pt. Its OO portion is closest to the Pt surface, with Pt–O distances of about 2 Å. The NO fragment is located about 3 Å above the Pt surface. Formation of this intermediate is exothermic starting either from adsorbed NO or O_2, reversing, for instance, the endothermicity of isolated O_2 adsorption at these high coverage conditions. In contrast, on an oxygen-free surface, OONO* is unstable to dissociation to 2O* and NO* by more than 3.1 eV. A similar intermediate has been proposed to account for the observed oxidation of NO to NO_2 over Cu-ZSM-5 catalysts [47].

Examination of O_2 adsorption and OONO* formation at O coverages intermediate to 0 ML and 0.66 ML shows similar trends in decrease in O_2 adsorption energy and binding enhancement by co-adsorption with NO. We represent a 1/4-ML O coverage using a $p(2 \times 2)$-O ordering and a 1/2-ML coverage with a $p(2 \times 1)$-O ordering. Coverage dependent binding energies and geometries are shown in Fig. 6. OONO* adsorption energies vary non-linearly with O coverage in the models chosen here. OONO* and O_2 adsorption are slightly diminished at 1/4 ML O and more significantly diminished at 1/2 ML O. In fact, we find OONO* (as well as NO_2) adsorbates to bind more weakly on the $p(2 \times 1)$-O surface than the $p(\sqrt{3} \times \sqrt{3})$-2O one, due to stronger local interactions with surface O in the former ordering. These binding energies are clearly a sensitive function both of O coverage and local adsorption environment.

The relative stability and connectivity of the OONO* intermediate are consistent with a role as an intermediate in the formation of NO_2. In fact, we find the reaction:

$$OONO* \rightarrow NO_2(g) + O'* \quad (5)$$

to be exothermic by 0.09 eV on the $p(\sqrt{3} \times \sqrt{3})$-2O surface. We denote the residual oxygen atom as O′* to emphasize the fact that this oxygen is left in an FCC site with six nearest neighbor oxygen and is thus particularly weakly bound. It can thus exothermically react with NO (g), by 1.97 eV, to form a second NO_2 (g)

$$NO(g) + O'* \rightarrow NO_2(g) + * \quad (6)$$

The DFT-calculated energy profiles for surface reactions of O_2 + 2 NO within one supercell at O coverages up to 2/3 ML

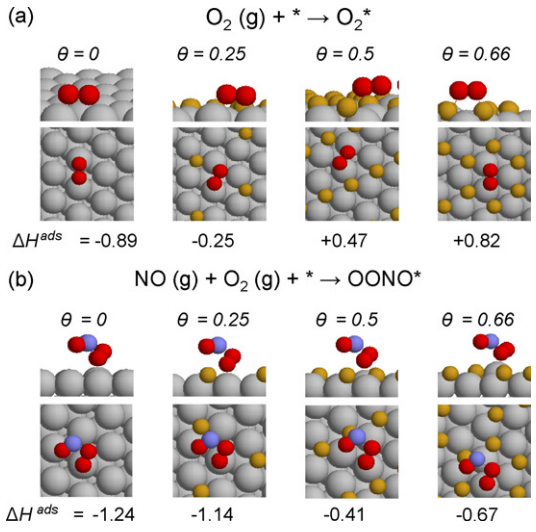

Fig. 6. O_2 independent adsorption (a) and co-adsorption with NO (b) as a function of coverage. Adsorption energies are given in eV and O coverages in ML.

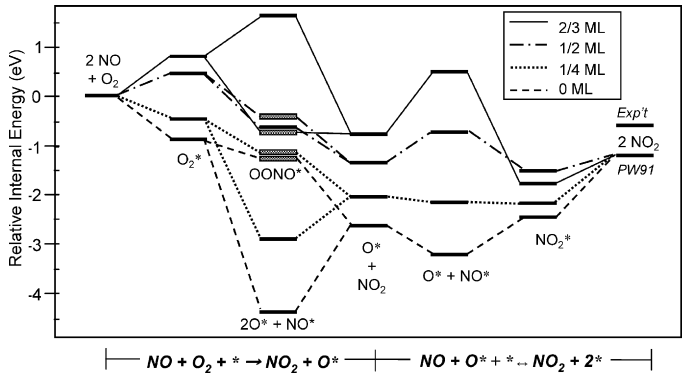

Fig. 7. Comparison of NO oxidation energetics as a function of O coverage. OONO* intermediates in the associative pathway are denoted with white bars.

are summarized in Fig. 7. The 0 ML dashed line illustrates the unfavorable surface energetic of NO oxidation at low surface coverage: while O_2 is readily dissociated on Pt(1 1 1) in this limit, the intrinsic Pt–O bond strength inhibits formation and desorption of NO_2. In contrast, at 2/3 ML O coverage, shown by the solid line, O_2 dissociation is strongly disfavored in isolation but assisted by interaction with NO. The high oxygen covered surface observed during catalytic NO oxidation is thus passivated towards O_2 dissociation, possibly opening up an NO-assisted O_2 dissociation pathway. Such a pathway involving intermediate OONO* is consistent with the first order dependence in O_2 concentration noted experimentally. Further, O_2 adsorption is the highest energy step on the energy profile, and the 0.8 eV endothermic energy is consistent with the observed activation energy for NO oxidation.

The intermediate coverage results in Fig. 7 illustrate the greater sensitivity of the O_2 dissociation energetic to surface coverage than for the associative pathway. The two pathways approximately coincide in energy near 0.5 ML O, where 2O* + NO* is just slightly preferred over OONO* and NO_2 formation is exothermic. Thus, both pathways may contribute to observed NO oxidation catalysis depending on reaction conditions. Actual contributions depend on the relative kinetics of these two pathways, as well as of surface diffusion, and are the topic of current investigation.

Finally, we note that the DFT/GGA model exaggerates the overall energy of NO oxidation (Reaction 1) by approximately 0.6 eV, characteristic of the GGA tendency to overestimate bond energies. Errors of similar magnitude may propagate into other binding energies but are unlikely to be large enough to alter the general trends noted here.

While the $p(\sqrt{3} \times \sqrt{3})$-2O ordering represents a lower oxygen coverage than that suggested by the *ex situ* AES experiments, based on the unfavorable energetics of dissociative oxidation and the favorable but weak binding of the associative OONO* intermediate found in the DFT simulations, it would appear to be at the high end of likely coverages for a catalytically active Pt(1 1 1) surface. Prediction of actual surface conditions requires calculation of adsorption energies at a wider range of coverages, as well as calculation of reaction barriers as a function of coverage. These are the topics of ongoing work.

5. Conclusions

The experimental results presented here support previous inferences that NO oxidation to NO_2 over Pt-based catalysts is faster on the Pt(1 1 1) crystal faces that dominate large crystallites. The observed reaction orders and activation energies on a Pt(1 1 1) single crystal are consistent with those previously noted for supported catalysts that take into account the inhibition due to NO_2. The turnover rate is the highest noted to date on a per exposed Pt atom basis, and within a factor of two of the rate on the largest particles studied [38]. This is in agreement with the idea that large, closed-packed crystalline Pt particles which are dominated by the closed-packed (1 1 1) facets are kinetically resistant to complete Pt oxidation under NO oxidation reaction conditions whereas small, amorphous Pt particles will oxidize to the bulk oxide and therefore become inactive. The inverse order dependence on NO_2 concentration, the high surface oxygen coverage observed with *ex situ* AES, and the absence of Pt oxides in XPS, all support a model in which catalysis occurs on an oxygen-covered metallic surface induced at least in part by the product NO_2. DFT simulations show that the energetic of a dissociative NO oxidation mechanism at a Pt(1 1 1) 2/3 ML O surface coverage – close to that observed experimentally – are highly unfavorable due to the very weak Pt–O* bonding on a highly covered surface. An associative OONO* intermediate is found to be moderately stable at 2/3 ML coverage and may provide a pathway for NO-assisted O_2 dissociation at this and lower coverages. Current experimental and computational work on this and on other low index faces of Pt will help to further clarify the roles of surface coverage and structure as they relate to NO oxidation mechanism and activity.

Acknowledgments

Support from the Department of Energy, Office of Basic Energy Sciences, Chemical Sciences, Geosciences, and Biosciences Division, under grants DE-FG02-06ER15830 and DE-FG02-03ER15408 is gratefully acknowledged, as are helpful conversations with Abhijit Phatak and computer time at the Center for Research Computing at the University of Notre Dame.

References

[1] F. Menil, V. Coillard, C. Lucat, Sens. Actuat. B: Chem. 67 (2000) 1.
[2] V.I. Pârvulescu, P. Grange, B. Delmon, Catal. Today 46 (1998) 233.
[3] W.S. Epling, L.E. Campbell, A. Yezerets, N.W. Currier, J.E. Parks, Catal. Rev. 46 (2004) 163.
[4] E. Xue, K. Seshan, J.R.H. Ross, Appl. Catal. B: Environ. 11 (1996) 65.
[5] J.-H. Lee, H. Kung, Catal. Lett. 51 (1998) 1.
[6] L. Olsson, B. Westerberg, H. Persson, E. Fridell, M. Skoglundh, B. Andersson, J. Phys. Chem. B 103 (1999) 10433.
[7] L. Olsson, H. Persson, E. Fridell, M. Skoglundh, B. Andersson, J. Phys. Chem. B 105 (2001) 6895.
[8] L. Olsson, E. Fridell, J. Catal. 210 (2002) 340.
[9] R. Marques, P. Darcy, P.D. Costa, H. Mellottee, J.-M. Trichard, G. Djega-Mariadassou, J. Mol. Catal. A: Chem. 221 (2004) 127.
[10] J. Despres, M. Elsener, M. Koebel, O. Kroecher, B. Schnyder, A. Wokaun, Appl. Catal. B 50 (2004) 73.

[11] S.S. Mulla, N. Chen, W.N. Delgass, W.S. Epling, F.H. Ribeiro, Catal. Lett. 100 (2005) 267.
[12] S.S. Mulla, N. Chen, L. Cumaranatunge, G.E. Blau, D. Zemlyanov, W.N. Delgass, W.S. Epling, F.H. Ribeiro, J. Catal. 241 (2006) 389.
[13] Y. Ji, T.J. Toops, U.M. Graham, G. Jacobs, M. Crocker, Catal. Lett. 110 (2006).
[14] W. Hauptmann, A. Drochnera, H. Vogela, M. Votsmeierb, J. Gieshoffb, Top. Catal. 42, 23 (2007) 157.
[15] R. Burch, S.T. Daniells, P. Hu, J. Chem. Phys. 107 (2002) 2902.
[16] S. Ovesson, B.I. Lundqvist, W.F. Schneider, A. Bogicevic, Phys. Rev. B 71 (2005) 115406.
[17] W.F. Schneider, in: V.H. Grassian (Ed.), Environmental Catalysis, CRC Press, New York, 2005.
[18] R.B. Getman, W.F. Schneider, J. Phys. Chem. C 111 (2007) 389.
[19] D. Mei, Q. Ge, M. Neurock, L.D. Kieken, J. Lerou, Mol. Phys. 102 (2004) 361.
[20] D. Dahlgren, J.C. Hemminger, Surf. Sci. 123 (1982) L739.
[21] D.H. Parker, M.E. Bartram, B.E. Koel, Surf. Sci. 217 (1989) 489.
[22] M.E. Bartram, R.G. Windham, B.E. Koel, Langmuir 4 (1988) 240.
[23] Y. Xu, W.A. Shelton, W.F. Schneider, J. Phys. Chem. B 110 (2006) 16591.
[24] Y. Xu, W.A. Shelton, W.F. Schneider, J. Phys. Chem. A 110 (2006) 5839.
[25] B.M. Weiss, E. Iglesia, Personal communication, 2007.
[26] H. Tsukahara, T. Ishida, M. Mayumi, NITRIC OXIDE: Biol. Chem. 3 (1999) 191.
[27] N.A. Saliba, C.P. Tsai, B.E. Koel, Surf. Sci. 419 (1999) 79.
[28] C.T. Campbell, G. Ertl, H. Kuipers, J. Segner, Surf. Sci. 107 (1981) 200.
[29] D.R. Monroe, R.P. Merrill, J. Catal. 65 (1980) 461.
[30] G. Kresse, J. Furthmüller, Comp. Mater. Sci. 6 (1996) 15.
[31] G. Kresse, J. Joubert, Phys. Rev. B 59 (1999) 1758.
[32] P.E. Blöchl, Phys. Rev. B 50 (1994) 17953.
[33] J.P. Perdew, Y. Wang, Phys. Rev. B 45 (1992) 13244.
[34] J.P. Perdew, J.A. Chevary, S.H. Vosko, K.A. Jackson, M.R. Pederson, D.J. Singh, C. Fiolhais, Phys. Rev. B 46 (1992) 6671.
[35] H.J. Monkhorst, J.D. Pack, Phys. Rev. B 13 (1976) 5188.
[36] T.H. Chilton, A.P. Colburn, Ind. Eng. Chem. 26 (1934) 1183.
[37] W. Hauptmanna, A. Drochnera, H. Vogela, M. Votsmeierb, J. Gieshoffb, Top. Catal. 42, 23 (2007) 157.
[38] M. Crocoll, S. Kureti, W. Weisweiler, J. Catal. 229 (2005) 480.
[39] J. Segner, W. Vielhaber, G. Ertl, Isr. J. Chem. 22 (1982) 375.
[40] NIST, NIST X-ray Photoelectron Specroscopy Database, Vol. 2007, NIST, 2006.
[41] H. Tang, A. Van der Ven, B.L. Trout, Phys. Rev. B 70 (2004) 045420.
[42] D.I. Jerdev, J. Kim, M. Batzill, B.E. Koel, Surf. Sci. 498 (2002) L91.
[43] J.F. Weaver, J.-J. Chen, A.L. Gerrard, Surf. Sci. 592 (2005) 83.
[44] A. Eichler, J. Hafner, Phys. Rev. Lett. 79 (1997) 4481.
[45] Z. Sljivancanin, B. Hammer, Surf. Sci. 515 (2002) 235.
[46] B. Liang, L. Andrews, J. Am. Chem. Soc. 123 (2001) 9848.
[47] W.F. Schneider, K.C. Hass, R. Ramprasad, J.B. Adams, J. Phys. Chem. B 101 (1997) 4353.